ACS OMEGA

http://pubs.acs.org/journal/acsodf

Article

High Light Outcoupling Efficiency from Periodically Corrugated OLEDs

Yu Zhang and Rana Biswas*

Cite This: *ACS Omega* 2021, 6, 9291−9301

Read Online

ACCESS | Metrics & More | Article Recommendations | Supporting Information

ABSTRACT: Organic light-emitting diodes (OLEDs) suffer from poor light outcoupling efficiency (η_{out} < 20%) due to large internal waveguiding in the high-index layers/substrate, and plasmonic losses at the metal cathode interface. A promising approach to enhance light outcoupling is to utilize internal periodic corrugations that can diffract waveguided and plasmonic modes back to the air cone. Although corrugations can strongly diffract trapped modes, the optimal geometry of corrugations and limits to η_{out} are not well-established. We develop a general rigorous scattering matrix theory for light emission from corrugated OLEDs, by solving Maxwell's equations in Fourier space, incorporating the environment-induced modification of the optical emission rate (Purcell effect). We computationally obtain the spectrally emissive power inside and outside the OLED. We find conformally corrugated OLEDs, where all OLED interfaces are conformal with a photonic crystal substrate, having triangular lattice symmetry, exhibit high light outcoupling η_{out} ~60−65%, and an enhancement factor exceeding 3 for optimal pitch values between 1 and 2.5 μm. Waveguided and surface plasmon modes are strongly diffracted to the air cone through first-order diffraction. η_{out} is insensitive to corrugation heights larger than 100 nm. There is a gradual roll-off in η_{out} for a larger pitch and sharper decreases for small pitch values. Plasmonic losses remain below 10% for all corrugation pitch values. Our predicted OLED designs provide a pathway for achieving very high light outcoupling over the full optical spectrum that can advance organic optoelectronic science and solid-state lighting.

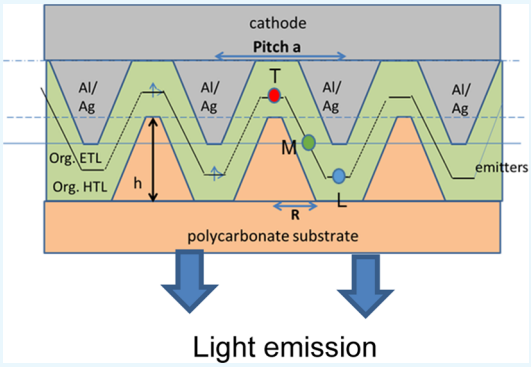

1. INTRODUCTION

Poor light extraction efficiency from organic light-emitting diodes (OLEDs) is among the leading problems facing their science and commercialization. Among the most commonly measured figures of merits for OLEDs is the electroluminescence external quantum efficiency η_{EQE}, which is the ratio of the number of photons emitted for each injected charge carrier, and is the product of the following factors[1,2]

$$\eta_{EQE} = \gamma \times \eta_{s/t} \times \eta_{\rho} \times \eta_{out} \quad (1)$$

Here, γ ıs the charge imbalance factor, $\eta_{s/t}$ is the ratio of singlet and triplet excitons, η_{ρ} is the radiative quantum efficiency of the emissive species, and η_{out} is the optical outcoupling factor. With the exception of η_{out}, the other factors can be optimized near ideal values (~1.0) by judicious OLED design. Although charge accumulation within the OLED reduces the charge imbalance factor γ below the ideal value of 1, charge imbalance can be reduced by optimization of electron and hole transport layers. The ratio of singlet to triplet excitons, $\eta_{s/t}$, is 0.25 in fluorescent materials and approaches 1 for current phosphorescent materials. The radiative quantum efficiency η_r represents how many of the spin allowed excitons decay through photon emission, as opposed to nonradiative decay channels through defects. Reducing defect density is critical for achieving a high η_r.

The outcoupling factor η_{out} is a purely *optical* factor representing the ratio of photons emitted to the air side, to all photons emitted *inside* the material. Clearly from 1, η_{EQE} can be significantly smaller than the outcoupling factor η_{out} since the product $\gamma \cdot \eta_{\sigma/\tau} \cdot \eta_{\rho}$ can be smaller than 1.

Intense effort is underway to improve the optical outcoupling.[3] Ray optics predicts that the fraction of light that can be emitted from a light source within a substrate of refractive index n is

$$\eta_{out} = 1 - \sqrt{1 - \frac{1}{n^2}} \approx \frac{1}{2n^2} \quad (2)$$

due to total internal refraction (TIR) within the high-index layer. For typical values of refractive indices of organic emissive layers ($n \sim 1.8$), this leads to an outcoupling factor $\eta_{out} \cong 17\%$ to the air side in traditional bottom-emitting OLEDs on glass substrates. Of the light generated in the organic layers, as much as half

Received: February 18, 2021
Accepted: March 12, 2021
Published: March 23, 2021

(depending on organic layer thickness) undergoes TIR at the ITO/substrate interface (as the refraction index $n(\mathrm{ITO}) \sim 2.0$ is larger than $n(\mathrm{glass}) \sim 1.5$) and is lost in subsequent reflections at the organic/metal and ITO/glass interfaces. A substantial fraction of the light undergoes similar TIR within the glass substrate and is waveguided to the edges of the glass where it appears as edge emission. In addition to waveguiding, there are plasmonic losses that increase when the emitting species is close to the cathode. The near-term technology target is to achieve an outcoupling η_{out} of 70%[4] by 2020.

Increasing light extraction from bottom-emitting OLEDs is being intensively studied by various approaches. The light that is waveguided in the *glass* substrate can be extracted by scattering centers within the glass substrate[5] or by micro-lens (μLA) arrays[6,7] at the air-glass side. It is particularly advantageous to have the μLA size *much* larger than the pixel to extract all of the waveguided light in glass, outside the pixel area.[7,8]

Various approaches to extract the large fraction of light trapped in the high-index organic/ITO layers include using low-index grids between the ITO and the organic layers—to diffract light from the ITO to the glass layer. Using a SiO_2 grid of refractive index $n(SiO_2) = 1.45$, in addition to a μLA on the blank glass side, an overall extraction efficiency of 34%, or an enhancement factor of 2.3, was reported.[9] An ultralow-index grid with $n_{\mathrm{grid}} \sim 1.13$ generated an extraction efficiency of ∼48% at 100 cd/m^2, i.e., an enhancement factor of nearly 3.[10] However, the light extraction efficiency $\eta_{\mathrm{out}} \sim 50\%$. Recently, a subelectrode-inverted μLA with pitch 10 μm, between the substrate and high-index layers, achieved $\eta_{\mathrm{EQE}} \sim 50\%$, which increased to ∼70% when an additional external μLA on the substrate−air interface was utilized.[11] Another promising approach was to conformally grow OLEDs on quasi-periodic buckled substrates, resulting in strong diffractive effects and an enhancement factor of ∼2.2, leading to $\eta_{\mathrm{out}} \sim 40\%$ and a nearly Lambertian light emission pattern.[12] OLEDs on buckled Al substrates with in-plane periods >1 μm show current and power efficiency enhancements of 1.6 and 1.9, respectively,[13] along with EQE enhancements of 20% when composite ETLs were utilized.[14] Random vacuum nano-hole arrays in the substrate in conjunction with a half-spherical lens as internal and external light extraction layers achieved ∼78% EQE and luminous efficacy of 164 lm/W when emissive dipoles were preferentially oriented in the in-plane direction.[15]

Fuchs et al.[16] found 1-d gratings fabricated in the ZnO:Al transparent bottom electrode, enhanced OLED EQE when the pitch was ∼0.71 μm, due to first-order Bragg scattering of WG modes to the emission cone. One-dimensional gratings in a photoresist layer underneath the bottom Ag/Al electrode in microcavity OLEDs showed[17] increased EQE from 15 to 17.5% for a grating period of 1.0 μm and a corrugation depth of 70 nm, and observed first-order and second-order Bragg scattering of the WG and SP modes into the emission cone. Altun et al.[18] fabricated corrugated OLEDs with a pitch of 530 nm and corrugation heights up to 100 nm, using a triangular lattice of pillar arrays in resin and indium-zinc oxide (IZO), and observed a 49% enhancement of the light extraction efficiency and 93% enhancement of the power efficiency. One-dimensional blazed gratings were used for internal corrugations of OLEDs, and 42% enhancement of the EQE of green OLEDs was observed.[19] Utilizing low-index LiF buffer layers were found to increase EQE to 61% in corrugated OLEDs.[20]

High-index polyimide substrates incorporated with titania nanoparticles and Ag nanowires showed enhanced EQE,[21] since the substrate better matches with the high-index organic emitting layers.

Although previous studies have identified internal periodic corrugations as a pathway for increased η_{out} from diffraction of the WG and SP modes, the majority of these studies have considered individual pitch values in the optical wavelength range. There has been limited understanding of the range of pitch values that would be optimal for outcoupling. Further, FDTD simulations define the structure in real space, and it is difficult to rescale the structure to another pitch value. Since our method is based on the scattering matrix in Fourier space, it offers the flexibility of easily changing the pitch and corrugation height as well as the ability to predict the critical parameter of the pitch in affecting η_{out}.

2. APPROACH

We develop a rigorous theoretical approach where integrated OLED substrates are periodically corrugated and the *entire* OLED stack is conformally grown on the patterned substrate, as has been demonstrated in recent experiments.[22] Photons are emitted isotropically by the emissive molecules, with a wave vector that lies on a sphere of radius $k = n(\mathrm{org})\omega/c$ (Figure 1).

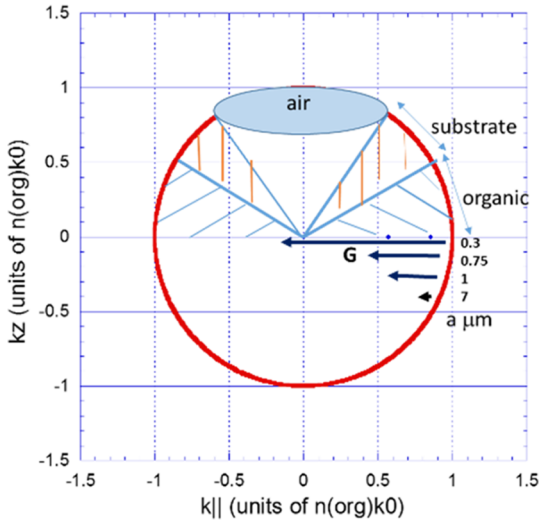

Figure 1. Photon momentum wave vectors emitted inside the OLED; identifying the regions of power emitted to air, trapped in the substrate and in the organic high-index layers. Magnitudes of **G** vectors at different corrugation pitch *a* are shown.

Since the parallel component of the wave vector ($k_{\parallel}$) is conserved in a planar OLED, only the small fraction of photons emitted in the narrow air cone defined by the critical angle $\theta_c = \sin^{-1}\left(\frac{1}{n(\mathrm{org})}\right) \sim 34°$ will be outcoupled to air ($n(\mathrm{org}) \sim 1.76$). The surface area of the air cone is precisely the fraction $\eta_{\mathrm{out}} = \frac{1}{2n^2}$ of the surface area of the sphere. Photons emitted with angles defined by $\frac{1}{n(\mathrm{org})} < \sin\theta < \frac{1}{n(\mathrm{sub})}$ are emitted to the substrate, whereas those with angles defined by $\frac{1}{n(\mathrm{sub})} < \sin\theta < 1$ are trapped in the high-index organic layers.

For OLEDs fabricated on a periodically corrugated substrate, the periodicity can diffract photons with a parallel wave vector **G** (Figure 1). A waveguided mode within the organic layer can be diffracted back to the air cone and outcoupled (Figure 1) such that $k_{\parallel} + \mathbf{G} = k_{\parallel}'$ lies *within* the air cone. Preliminary experiments

https://doi.org/10.1021/acsomega.1c00903
ACS Omega 2021, 6, 9291−9301

on corrugated OLEDs[16] indicate substantial enhancements of $\eta_{EQE} \sim 50\%$, suggesting even higher possible values of η_{out}. It is the goal of this study to predict what types of periodic corrugations, i.e., their pitch and height, can lead to optimal enhanced outcoupling.

3. THEORY OF LIGHT EMISSION FROM OLEDS

We develop a theoretical rigorous scattering matrix framework for light emission from periodically corrugated OLEDs. Our goal is to develop computational approaches to model the enhanced outcoupling and the emission from OLEDs fabricated on integrated, periodically corrugated substrates. Since η_{out} cannot be measured directly, modeling the losses and η_{out} is critical for advancing OLED science and guiding the fabrication of optimum integrated substrates.

We adapted the scattering matrix (SM) approach[23] that has been extremely valuable in computing the reflection, transmission, and absorption of photonic crystals and periodically corrugated solar cells.[24] There is a critical distinction between the SM approach and the widely employed transfer matrix approach utilized by Furno et al.[25] for calculating light emission from *flat* OLEDs. The dipole excitation source within the emissive layer emits with amplitude a_{inc}^{+} and a_{inc}^{-} in forward and backward directions (Figure 2). The SM approach computes the

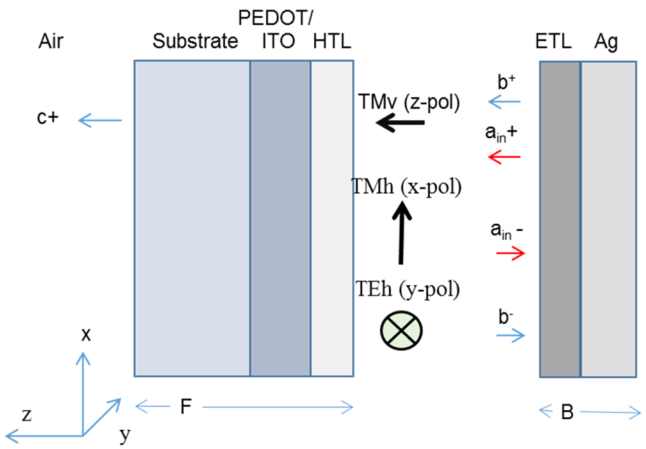

Figure 2. Schematic showing the three dipole polarizations in the emissive layer of a flat OLED. Transverse magnetic (TM) modes have electric field (**E**) in the plane of the figure. The transverse electric (TE) mode has **E** perpendicular to the plane.

amplitudes (b^+, b^-) of the *total* electric fields for waves propagating in the OLED in the positive and negative directions (Figure 2). The scattering matrices (F) for the substrate/ITO or PEDOT:PSS/HTL stack and the ETL/Ag cathode stack (B) *already include multiple scattering effects*, similar to the formalism employed by Egel and Lemmer.[26] In contrast, the previous transfer matrix theory by Furno et al.[25] uses the single-pass reflectance coefficients a^+ and a^- from the top and bottom of the OLED stack. Such reflectances are not directly calculated by the SM approach, and hence we cannot directly use the expressions of Appendix A in Furno et al.[25] for the power emitted by the OLED, in our approach.

Thus, we re-derive the theory of OLED emission based on the scattering matrix using ref. 25 as guidance. The fields in the emissive layer are the sum of the incident field a_{in} and the total reflected field b, traveling in both directions[20] (Figure 2). For ease of visualization, we first describe the emission from a flat OLED stack and then generalize to the corrugated case.

The power emitted *within* the OLED arises from the three dipole polarizations corresponding to z, x, and y orientations of the dipole and are considered separately below and discussed in the Supporting Information (SI).

3.1. Flat OLEDs. *3.1.1. Transverse Magnetic Vertical (TMv) Polarization (z-Polarization).* The power emitted by the vertical electric dipole (oriented in the z direction), or the TMv polarization P(TMv), is given by the general OLED emission theory of Sullivan and Hall[27] or in terms of the total fields $\mathcal{A}$ within the OLED emissive layer. We relate $\mathcal{A}$ to the SM fields b through

$$P(\mathrm{TMv}) = \frac{3}{2}\int_0^\infty \mathrm{d}u \frac{u^3}{\sqrt{1-u^2}}\{\mathcal{A}^{-e} + \mathcal{A}^{+e}\} = \frac{3}{2}\int_0^\infty \mathrm{d}u \frac{u^3}{\sqrt{1-u^2}}\{1 + b_i^+ + b_i^-\} \quad (3)$$

where u is the scaled wave vector inside the OLED ($u = k_{||}/(n(\mathrm{org})k_0)$).

3.1.2. Transverse Electric Horizontal (TEh) Polarization (x-Polarization). The power emitted in TEh modes is

$$P(\mathrm{TEh}) = \frac{3}{4}\int_0^\infty \mathrm{d}u \frac{u}{\sqrt{1-u^2}}\{1 + b_i^+ + b_i^-\} \quad (4)$$

3.1.3. Transverse Magnetic Horizontal Polarization (TMh) Modes (y-Polarization). The TMh modes have an odd integrand[19,21] (e.g., eq. 46 in ref 19) and the power emitted in TMh modes after adding the incident field is

$$P(\mathrm{TMh}) = \frac{3}{4}\int_0^\infty \mathrm{d}u \frac{u(1-u^2)}{\sqrt{1-u^2}}\{1 + b_i^- - b_i^+\} \quad (5)$$

We utilize eqs 3−5 for the numerical results for the three polarizations (Figure 2). The total emitted power is

$$P(\mathrm{tot}) = P(\mathrm{TMv}) + P(\mathrm{TMh}) + P(\mathrm{TEh}) = \int_0^\infty \mathrm{d}u\, P(u) \quad (6)$$

3.2. Corrugated OLEDS. We develop a scheme for light emission in a periodically corrugated OLED with pitch a and corrugation height h (Figure 3). The *two-dimensional* periodic corrugation in the x, y plane is described by reciprocal lattice vectors **G**, which for the triangular lattice are

$$\mathbf{G}_1 = \frac{2\pi}{a}\left(1, -\frac{1}{\sqrt{3}}\right);\ \mathbf{G}_2 = \frac{2\pi}{a}\left(0, \frac{2}{\sqrt{3}}\right) \quad (7)$$

Recent experiments and electron microscopy characterization[16] showed that OLEDs fabricated on corrugated substrates grow conformally with every layer in the OLED having the same pitch, and similar corrugation height, indicating that conformal OLEDs are most relevant for simulation.

Although the conical protrusions are rounded in the fabricated substrates,[16] we have approximated them in simulations as slanted cones with flat tops (Figure 3). The emissive dipoles form circular contours around the conical substrate corrugations (Figure 3b), leading to a complex emissive zone that follows the profile of corrugations. As we discretize the OLED into different slices in the z direction, the emissive zones change their cross-sectional area (Figure 3).

https://doi.org/10.1021/acsomega.1c00903
ACS Omega 2021, 6, 9291−9301

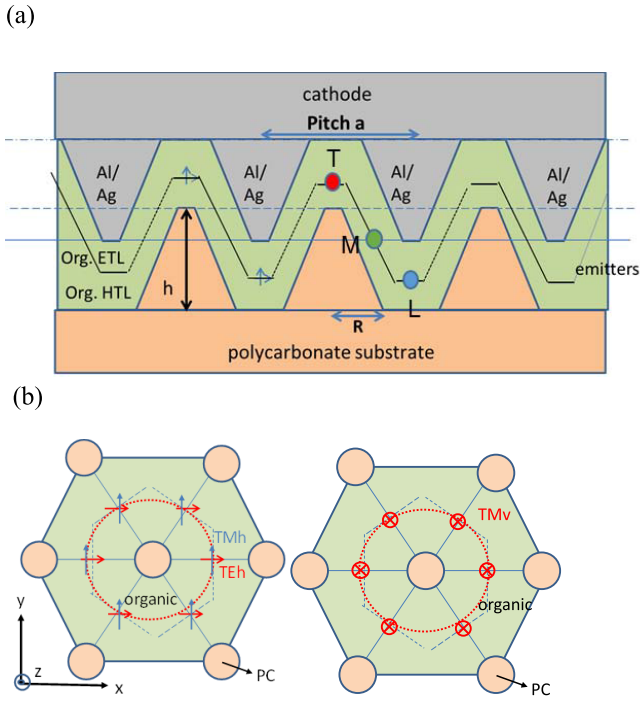

Figure 3. (a) Schematic structure of the corrugated OLED in a two-dimensional projection. Three representative positions of the dipole with different heights: low (L), mid (M), and top (T). (b) Positions of the dipole emittters in a planar *x*, *y* cross section of the OLED. The horizontal polarizations of the dipole (TMh, TEh) and the vertical polarization (TMv) are indicated, with the convention that *xz* is the emission plane.

The traveling waves *inside* the OLED have amplitudes $b^+(u,\mathbf{G})$ and $b-(u,\mathbf{G})$ in the $+z$ and $-z$ directions, whereas the emitted intensity in air is described by the amplitude $c^+(u,\mathbf{G})$. The fields depend on $u = k_{||}/n(\text{org})k_0$, the scaled dimensionless parallel component of the wave vector inside the OLED, and $\mathbf{G}$, which indexes the Fourier components. The corrugated OLED requires n_G Fourier components to describe the spatially varying nature of both the electric fields and the corrugation. Following the SM formalism (derived in the SI), the reflected field amplitudes are

$$b^+(u,\mathbf{G}) = (1 - \text{B21F21})^{-1}(\text{B21a}_{\text{in}}^- + \text{B21F21a}_{\text{in}}^+) \quad (8)$$

$$b^-(u,\mathbf{G}) = (1 - \text{F21B12})^{-1}(\text{F21a}_{\text{in}}^+ + \text{F21B12a}_{\text{in}}^-) \quad (9)$$

The scattering matrices (B21, F21) are $n_G \times n_G$ matrices. This gives the fields $b^+(u,\mathbf{G})$ and $b^-(u,\mathbf{G})$ in the organic emissive layer. The amplitude of the emitted fields in air is (SI)

$$\begin{aligned} c^{+e} &= c^+(u,\mathbf{G}) \\ &= \text{F11}a_{\text{in}}^+ + \text{F11}(1 - \text{F21B12})^{-1}(\text{F21}a_{\text{in}}^+ + \text{F21B12}a_{\text{in}}^-) \end{aligned} \quad (10)$$

The emissive dipole layer follows a corrugated profile conformal with the substrate corrugation. The dipole emission rate Γ_s is a function of the lateral position ($\mathbf{x} = (x,y)$) in the emissive layer. $H(\mathbf{x})$ denotes the locations of the dipole in the plane, describing the circular ring-like contours (Figure 3). $H(\mathbf{x})$ has Fourier components $H(\mathbf{G})$

$$\begin{aligned} H(x) &= \sum_{\mathbf{G}} \exp(\mathbf{iG}\cdot x)H(\mathbf{G}) \text{ or } H(x) \\ &= \int \mathrm{d}x \exp(-\mathbf{iG}\cdot x)H(\mathbf{G}) \end{aligned} \quad (11)$$

We integrate the emission from the (x,y) positions of the dipole. The power in the corrugated OLED for the three polarizations is convoluted with the positions of the dipoles in the emissive layer to be (SI)

$$\begin{aligned} P(\text{TMv}) &= \frac{3}{2}\int_0^\infty \mathrm{d}u \frac{u^3}{\sqrt{1-u^2}} \left\{1 + \sum_{\mathbf{G}} [b_i^+(u,\mathbf{G}) + b_i^-(u,\mathbf{G})]H(\mathbf{G})\right\} \\ P(\text{TMh}) &= \frac{3}{4}\int_0^\infty \mathrm{d}u \frac{u(1-u^2)}{\sqrt{1-u^2}} \left\{1 + \sum_{\mathbf{G}} [b_i^-(u,\mathbf{G}) + b_i^+(u,\mathbf{G})]H(\mathbf{G})\right\} \\ P(\text{TEh}) &= \frac{3}{4}\int_0^\infty \mathrm{d}u \frac{u}{\sqrt{1-u^2}} \left\{1 + \sum_{\mathbf{G}} \{b_i^+(u,\mathbf{G}) + b_i^-(u,\mathbf{G})\}H(\mathbf{G})\right\} \end{aligned} \quad (12)$$

3.3. Power Emitted in Air for Corrugated OLEDs. To simulate the outcoupled power, we have generalized the field components $c^+(u)$ for planar OLEDs to the Fourier components $c^+(u,\mathbf{G})$ for corrugated OLEDs. Only field components propagating in the positive $+z$ direction (i.e., outward from air) exist for these emitted modes. There is no incident field in the air so that the constant term (in eqs 3−5) is absent. The scattering matrix simulation computes $c^+(u,\mathbf{G})$ for TMv, TMh, and TEh (z,y,x) polarizations to yield the emitted power

$$\begin{aligned} P^{\text{air}}(\text{TMv}) &= \frac{3}{2}\int_0^\infty \mathrm{d}u \frac{u^3}{\sqrt{1-u^2}}\{\mathcal{A}^{+e}\} \\ &= \frac{3}{2}\int_0^\infty \mathrm{d}u \frac{u^3}{\sqrt{1-u^2}}\left\{\sum_{\mathbf{G}}^{k_z^2>0} c_{\text{TMv}}^+(u,\mathbf{G})\right\} \end{aligned} \quad (13)$$

$$P^{\text{air}}(\text{TMh}) = \frac{3}{4}\int_0^\infty \mathrm{d}u \frac{u(1-u^2)}{\sqrt{1-u^2}}\left\{\sum_{\mathbf{G}}^{k_z^2>0} c_{\text{TMh}}^+(u,\mathbf{G})\right\} \quad (14)$$

$$P^{\text{air}}(\text{TEh}) = \frac{3}{4}\int_0^\infty \mathrm{d}u \frac{u}{\sqrt{1-u^2}}\left\{\sum_{\mathbf{G}}^{k_z^2>0} c_{\text{TEh}}^+(u,\mathbf{G})\right\} \quad (15)$$

The sum over Fourier components $\mathbf{G}$ is for propagating modes, where $k_z^2 > 0$, where

$$k_z^2 = \left(\frac{\omega}{c}\right)^2 - (u + \mathbf{G}_x)^2 - \mathbf{G}_y^2 \quad (16)$$

The total emitted power is

https://doi.org/10.1021/acsomega.1c00903
ACS Omega 2021, 6, 9291−9301

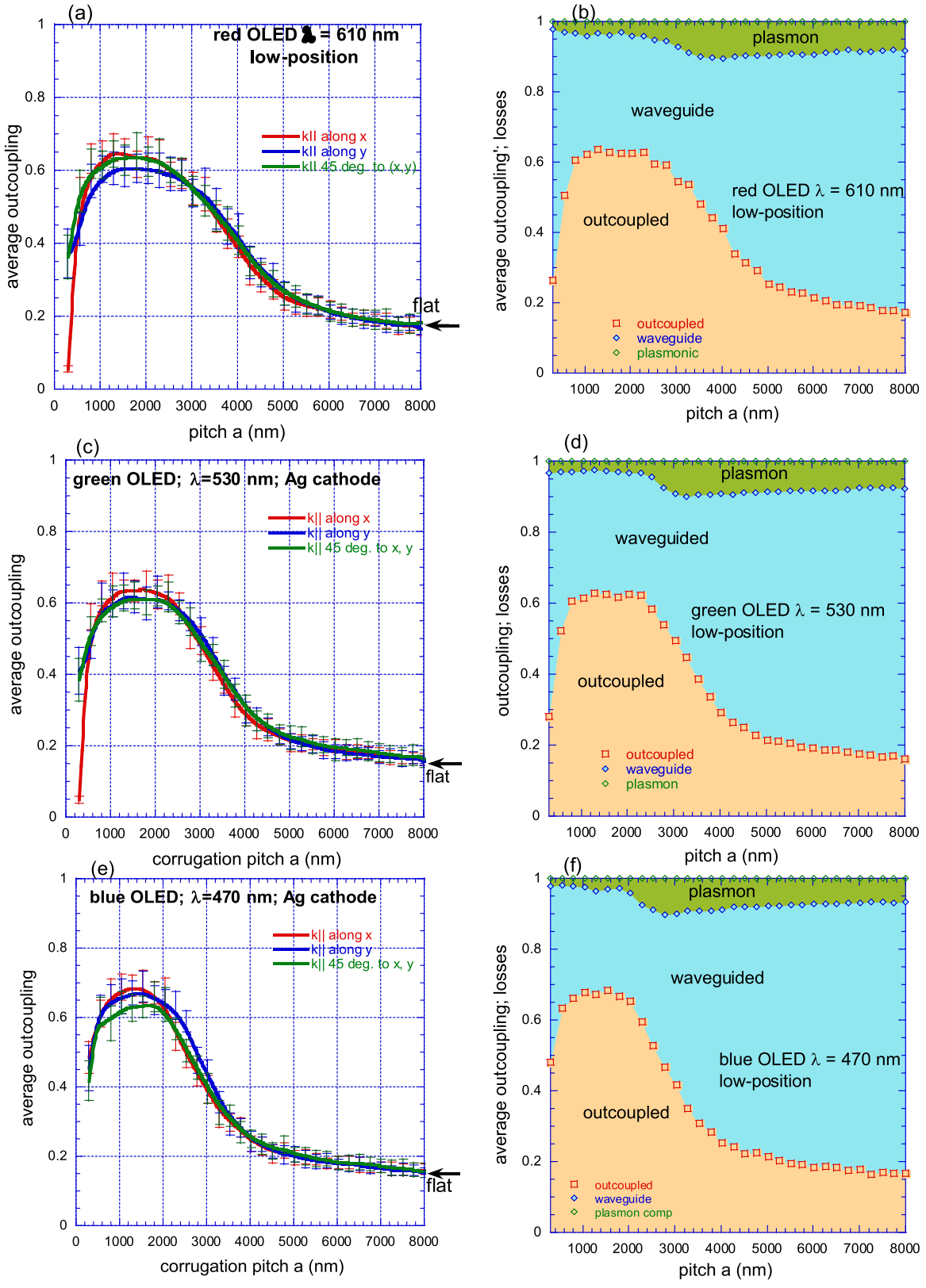

Figure 4. (a) Simulated corrugated OLED outcoupling as a function of corrugation pitch *a*, for a fixed corrugation height h of 200 nm and a red wavelength of 610 nm. The parallel wave vector $k_{||}$ is along *x*, *y*, and 45° to *x* or *y* axes. The average outcoupling is taken over ETL thickness *d* (ETL) from ±10 nm around an average value of $\lambda/4n(\mathrm{org})$, and the errors bars indicate the variance. (b) Division of power into outcoupled modes, waveguided losses, and plasmonic losses. The different $k_{||}$ directions have been averaged. (c, d) Green (530 nm); (e, f) blue (470 nm). The outcoupling for the flat OLED is indicated.

https://doi.org/10.1021/acsomega.1c00903
ACS Omega 2021, 6, 9291−9301

$$P^{air}(\text{tot}) = P^{air}(\text{TMv}) + P^{air}(\text{TMh}) + P^{air}(\text{TEh}) = \int_0^\infty du\, P^{air}(u) \quad (17)$$

4. RESULTS

As in the experiments,[16] we utilize a polycarbonate substrate (n = 1.58) that is better index-matched to the high-index organic layers, thereby reducing waveguiding in the organic layers and improving outcoupling, relative to glass substrates. We use experimental values of the wavelength-dependent complex refractive indices $n(\lambda) = n_1(\lambda)+in_2(\lambda)$ for silver[28] and ITO,[22] and spectroscopic ellipsometric measurements for typical organic layers[29] using the same $n(\lambda)$ for the ETL and HTL. We keep the HTL thickness constant and vary the thickness of the ETL layer (Figure 3). The plasmonic losses are very large for flat OLEDs with thin ETLs when the emitter is close to the cathode, but decrease as the ETL thickness increases. The flat OLED results are summarized in the SI. We found that $n_G \sim 61$ Fourier components (**G**-vectors) offer good convergence.

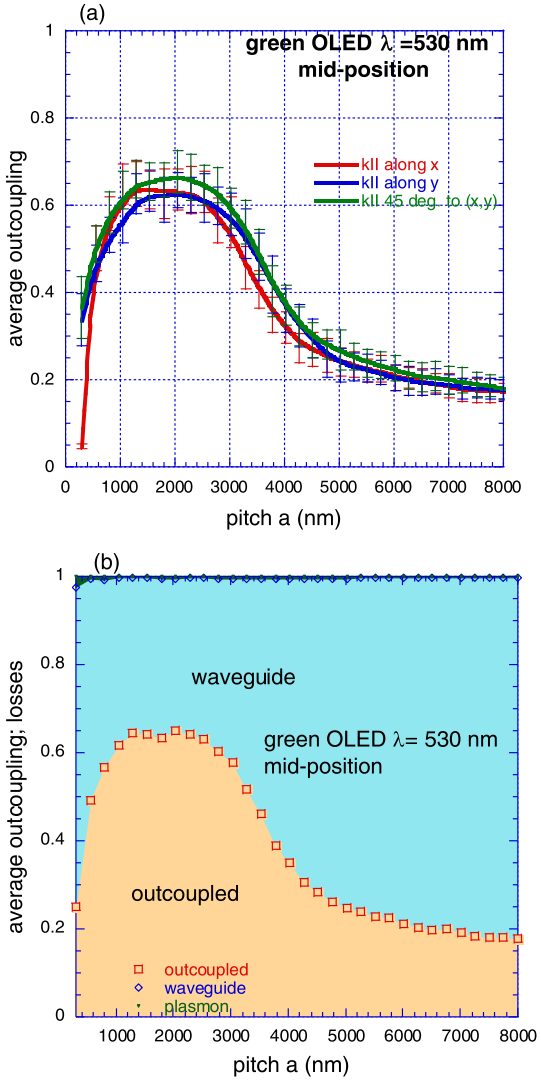

Figure 5. (a) Outcoupling as a function of pitch a for different $k_{||}$ values, at the mid-position (M) of dipoles. (b) Averaged outcoupling and losses for the mid-position. Conventions follow Figure 4.

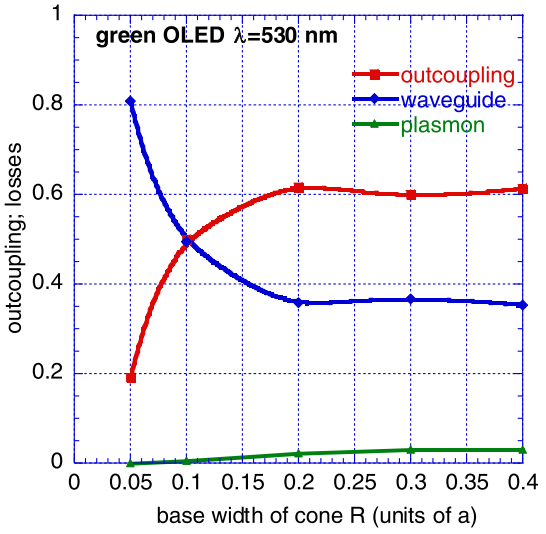

Figure 6. Variation of the outcoupled, waveguided, and plasmonic components of the power to the width R of the base of the cones. The aspect ratio of the cones is kept constant (R_t/R = 0.2). Results are the average for pitch values of 800−2500 nm around the optimal pitch range, at the low position (L).

We simulate a conformally corrugated OLED with an optically thick polycarbonate substrate, on which there are periodic corrugations of height h (Figure 3). All of the layers of the conformal OLED have corrugations of the same height, resulting in a complex three-dimensional emissive region that follows the corrugation contour (Figure 3). The OLED stack is polycarbonate (PC; n = 1.58)/corrugations in PC (height h nm, pitch a)/HTL (d(HTL) nm)/emissive region/ETL d nm/Ag cathode. Since the optimum ETL thickness is near a quarter wavelength $\lambda/4n$(org), we calculate η_{out} for a range of ETL thickness (typically ∼ 20 nm) around this value. For green (λ = 530 nm, n(org) ∼ 1.76), OLEDs $\lambda/4n$(org) ∼ 75 nm, when we account for a ∼ 10 nm penetration of the electric field inside the cathode, d ∼ 65 nm. Accordingly, we use a range of d ∼ 55 to 75 nm for the ETL. Similarly, the expected HTL thickness is near $\lambda/2n$(org) to maximize the field into the thick substrate.[19]

We simulate η_{out} as a function of the corrugation pitch a and height h, for three representative wavelengths: 610 nm (red), 530 nm (green), and 470 nm (blue). The numerical implementation of the theory is detailed in the SI. Since recent experiments[16] indicate optimal corrugation heights h ∼ 200 to 300 nm, we initially show results for h = 200 nm. Since the triangular lattice of corrugations is anisotropic, it was necessary to simulate different planes for the light emission. Accordingly, we selected the parallel component of the photon wave vector $k_{||}$ along the (i) x-axis (ii) y-axis, and (iii) line 45° to the x and y axes, corresponding to light emission in the xz, yz planes, and the plane bisecting the xz, yz planes. We initially selected the dipole emission from the ring-like contour closest to the substrate ("low" position).

For each $k_{||}$, our simulation shows a broad maximum η_{out} ∼ 0.6 to 0.65 for pitch a ∼ 1000 to 2500 nm (Figure 4a,c,e). This provides an enhancement factor >3 from the flat OLED, where η_{out} ∼ 0.2. Although the three orientations have similar results at larger a, $k_{||}$ along the x orientation has weaker η_{out} for a < 500 nm (Figure 4). We averaged the orientations to estimate the averaged η_{out} (Figure 4b,d,f), which also shows optimal η_{out} ∼ 0.6 to 0.65 for a ∼1000 to 2500 nm. At a large pitch a, η_{out}

https://doi.org/10.1021/acsomega.1c00903
ACS Omega 2021, 6, 9291−9301

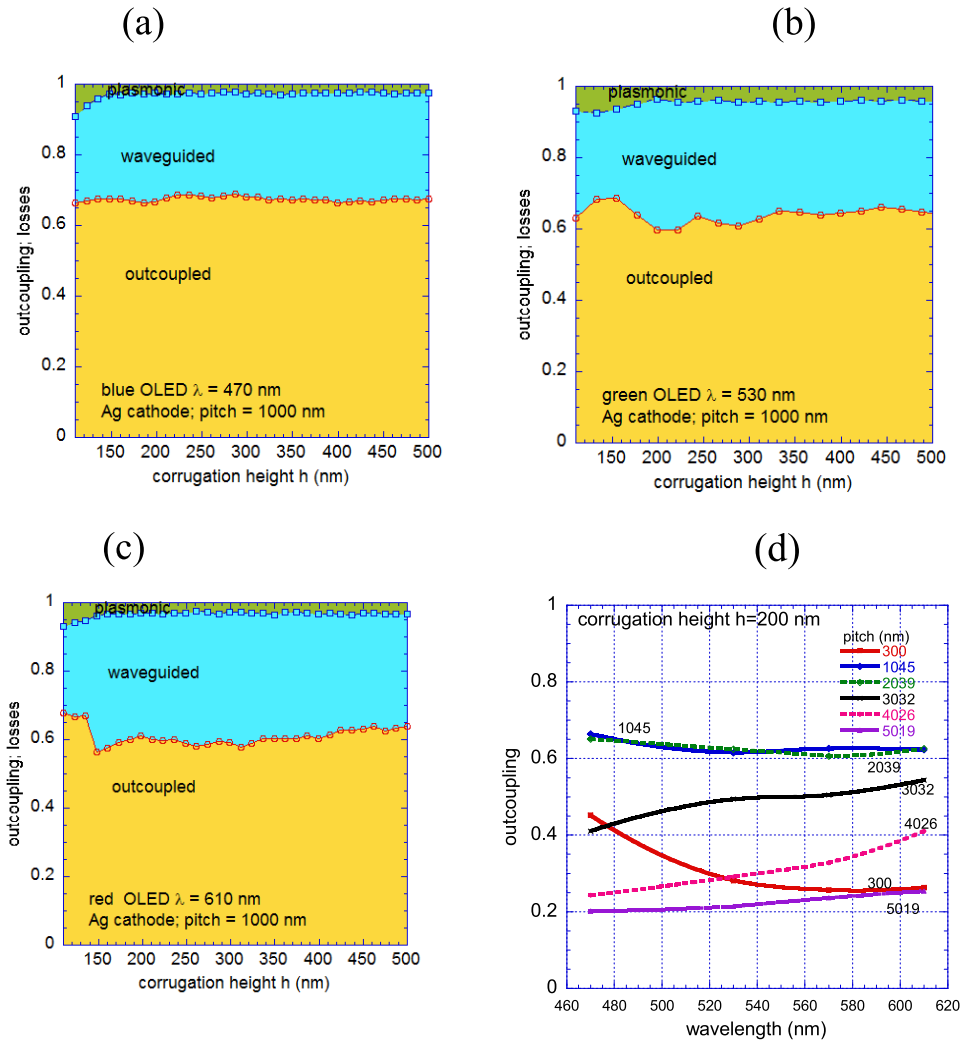

Figure 7. (a) Division of power into outcoupled, waveguided, and plasmonic losses for a blue OLED (λ = 470 nm) as a function of corrugation height, from 100 to 500 nm for the low position (L). (b) Results for a green OLED (λ = 530 nm). (c) results for a red OLED (λ = 610 nm). (d) Dependence of the outcoupling on wavelength for different pitch arrays.

decreases smoothly toward the flat limit ($\eta_{out} \sim 0.2$). η_{out} decreases sharply at a smaller pitch $a < 500$ nm, also approaching the flat OLED limit. By computing the emitted spectral power $P_{air}(u)$ and comparing with the spectral power inside the OLED $P_{in}(u)$, we estimated the fraction of power confined to waveguided modes (in both the high-index organic and substrate modes) and trapped surface plasmon modes at the organic−cathode interface (Figure 4). Plasmonic losses are sharply reduced by the corrugations, and are 5−10%. The waveguiding losses are ∼30% near the optimal pitch a (1−2.5 μm), but increase significantly at larger a and increase sharply at small a < 500 nm. At large a, as the corrugated structure approaches the flat limit, the predominant losses are from waveguided modes (70%) and smaller plasmonic loss (∼10%), with outcoupling approaching the flat $\eta_{out} \sim 0.2$.

We next simulate η_{out} for ring of dipoles in between the apex and base of the nanocones, aligned with the tip of the metal cathode ("mid-position:M," Figure 3). η_{out} shows similar trends as for the low position, including the optimal pitch range 1000−2500 nm with a maximum $\eta_{out} \sim 0.6$ to 0.65 (Figure 5, λ = 530 nm). The waveguiding losses are larger, and the plasmonic losses are negligible. The relative weighting of the mid-position (M) and low position (L) depend on the radius of the ring of dipole emitters (R_{mid}, R_{low}). For the experimental structure of nanocones with rounded tops,[22] there is a negligible density of dipoles in the top (T) position, which need not be considered as a first approximation. For near-optimal OLED structure with pitch $a \sim 1000$ nm, h = 200 nm and $R_{mid}/R_{low} \sim 0.72$ so that the weighting of the mid-position is $w_m \sim 0.42$ and the dominant low position is $w_l \sim 0.58$.

The structural parameters of the nanocone array are critical to guide fabrication.[22] We simulate the variation of the outcoupling with the variation of the bottom width (R) of the cones, in Figure 6. Results for the average values over the best ranges of pitch $a \sim$ 800 to 2500 nm are shown (Figure 6). We find that as the bottom width R is made smaller, i.e., the cones become very narrow, the outcoupling decreases with a corresponding increase in the waveguided component. For consistency, the same aspect ratio of the cones is utilized, in which the top width (R_t) and bottom width (R) have the fixed ratio, i.e., $R_t/R = 0.2$. The cone base widths $R > 0.2a$ are in a good range for achieving good light outcoupling.

The corrugation height is an important parameter for experimental fabrication.[22] When the corrugation height h is varied (near-optimal pitch a = 1000 nm), η_{out} and waveguiding/plasmonic losses are relatively insensitive to h (Figure 7a; for $h >$

https://doi.org/10.1021/acsomega.1c00903
ACS Omega 2021, 6, 9291−9301

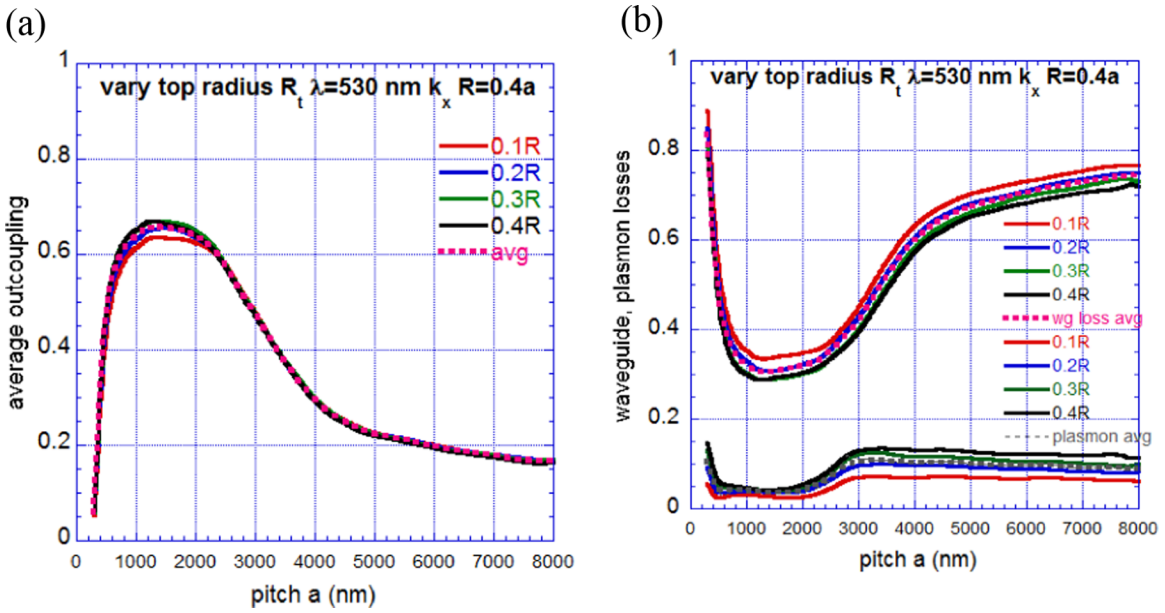

Figure 8. (a) Outcoupling as a function of pitch a for different cone top widths R_t as a ratio of the base radius R. (b) Waveguided and plasmonic losses as a function of a for different cone top widths R_t. Results are for green OLEDs at the low position (L) and for $k_{||}$ along x, following the conventions of Figure 4b.

100 nm) for blue and green OLEDs (Figure 7b) or red OLEDs (Figure 7c). η_{out} is slightly lower for red wavelengths. The diffraction of waveguided and plasmonic modes into the air cone is insensitive to the corrugation height, which is highly beneficial for experiments, since small experimental variations in h should not influence η_{out}. Although shown for the low position (L) for λ = 530 nm, these results are similar for other wavelengths and optimal pitch values. There is a negligible density of dipole emitters at the top of the nanocone.

We simulate η_{out} (λ) as a function of the wavelength for fixed values of the pitch a (Figure 7d). Near optimal $a \sim 1000$ to 2500 nm, η_{out} decreases slightly as the wavelength increases. At a small pitch ($a \sim 300$ nm), η_{out} decreases significantly as λ increases-showing increased η_{out} for blue OLEDs, relative to green and red. At a large pitch, η_{out} is smaller but increases weakly as λ increases. These factors are important for designing white OLEDs with different λ emitters.

We simulated the dependence of the outcoupling and losses as a function of the base angle of the cone (Figure 8). Results are shown (Figure 8) for a green OLED (λ = 530 nm), for a base radius $R = 0.4a$ and $k_{||}$ along x—corresponding to the parameters in Figure 4b. Near the optimal pitch (1000−2000 nm), η_{out} slightly decreases by ∼5% for narrow cones ($R_t = 0.1R$), relative to the wider top ($R_t = 0.4R$). η_{out} is insensitive to R_t for larger pitch values. The waveguiding losses somewhat increase (by ∼17%), whereas the plasmon losses slightly decrease for narrow cones ($R_t = 0.1R$) relative to wider top cones ($R_t = 0.4R$). At pitch a = 1000 nm, the base angles of the cones change from 29 to 45° as R_t varies from $0.1R$ to $0.4R$.

To understand the anisotropy of the light emission and the optimal pitch, we project the air emission cone, substrate waveguided zone, and organic waveguided zone in k-space on the reciprocal lattice of the triangular array. The substrate and organic waveguided modes are defined by rings of radii $k_{||} = n(\text{subs})k_0$ and $k_{||} = n(\text{org})k_0$, respectively. Plasmon modes reside beyond the organic ring $k_{||} > n(\text{org})k_0$ (Figure 9). We first examine a small pitch a = 300 nm (Figure 9a). When $k_{||}$ is along y, there is a primitive reciprocal lattice vector $\mathbf{G_2}$ (along y—blue vector) to diffract both the surface plasmon modes and the organic/substrate waveguided modes back to the air cone, where the light is outcoupled, by first-order diffraction. However, for $k_{||}$ along x, the first-order diffraction through $\mathbf{G_1}$ (vector at 30° to the x axis) diffracts the organic waveguided or plasmon mode to the substrate cone, but not to the air cone. The $\mathbf{G}$ vectors are too large for first-order diffraction to be effective, leading to anisotropy between the xz and yz emission planes at a very small pitch.

We show emission cones for a green OLED near the optimal pitch range a = 750 nm in Figure 8b. First-order diffraction through $\mathbf{G_1}$, $\mathbf{G_2}$ vectors have the right magnitude to diffract waveguided and plasmon modes back to the air cone for emission in the xz plane ($k_{||}$ along x) and yz plane ($k_{||}$ along y), indicating more isotropic emission, confirmed by the outcoupling results in Figure 4. For a much larger pitch $a \gg \lambda$ (Figure 9c), the $\mathbf{G}$ vectors are much smaller than the width of the air cone $|\mathbf{G}| \ll 2\pi/\lambda$. Very high orders of diffraction are then needed to diffract waveguided or plasmonic modes to the air cone, and this is a weak process (Figure 9c). As illustrated for a large pitch a = 4000 nm (Figure 9c), first-order diffraction by vectors ($\mathbf{G_1}$, $\mathbf{G_2}$) cannot diffract modes from the organic cone or plasmon regions to the air cone. This explains the decrease of η_{out} with a large pitch and η_{out} approaching the flat OLED value (Figure 5a) at large a.

5. DISCUSSION

Our simulated η_{out} variation with pitch a (Figure 4) can be compared to earlier results[30] for external μLAs on glass substrates. FDTD and ray-tracing simulations for triangular lattices of close-packed μLAs, found lens diameters ($d = a$) greater than ∼2 μm, generated $\eta_{out} \sim 0.32$, compared to $\eta_{out} \sim$ 0.17 to 0.2 for flat OLEDs. When the μL diameter $d < 1$ μm approached optical wavelengths, η_{out} decreased rapidly[24] similar to our results (Figure 4). This roll-off at a small pitch has some similarities to our simulations, which occurs here at $a \sim 0.5$ μm—smaller than in the μLA simulations, due to (i) the higher

https://doi.org/10.1021/acsomega.1c00903
ACS Omega 2021, 6, 9291−9301

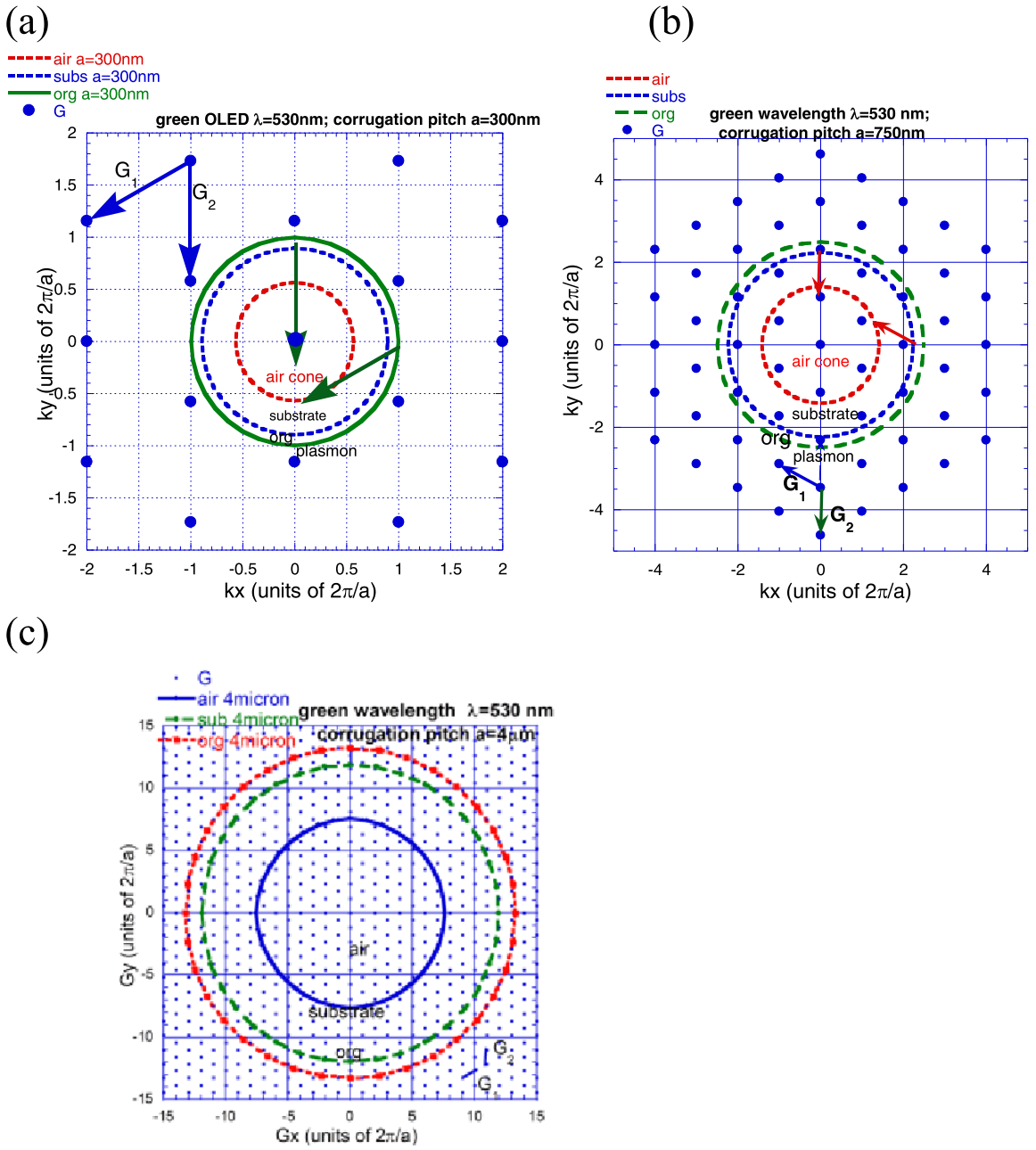

Figure 9. (a) Reciprocal lattice of the triangular array (blue circles) with the primitive reciprocal lattice vectors $\mathbf{G}_1$, $\mathbf{G}_2$ shown. Superimposed on this scale are the air emission cones for air, substrate, organic, and plasmon. First-order diffraction by $\mathbf{G}_1$, $\mathbf{G}_2$ are shown. Diffraction in the *y*-direction $\mathbf{G}_2$ corresponding to the *y*−*x* emission plane is more effective in diffraction than in the *xz* emission plane. (b) Similar plot for a pitch a = 750 nm close to the optimal range. (c) Plot for a large pitch a = 4000 nm.

index of the corrugated organic layer ($n \sim 1.75$ to 1.8) here than the glass μLA ($n \sim 1.45$[24]) and (ii) the decrease of first-order diffraction efficiencies at a small a. However, η_{out} is relatively flat out to a larger pitch a for μLAs, which is different from our results. μLAs at the air−substrate interface in addition to internal corrugations will likely enhance η_{out} further.

Our simulated outcoupling with periodic corrugations can be compared to previously studied random corrugations[11−15] that display local order in the nearest-neighbor shell. Similar to our results, OLEDs patterned with a complex graded photonic super crystal were theoretically predicted to have efficiencies >70%,[31] with the triangular lattice outperforming the square lattice. Periodic arrays with dual periodicities may be another promising future direction for OLEDs. Microcavity white OLEDs with corrugated (Al, Au) electrodes having dual periodicities of 225 and 325 nm tuned for blue and orange wavelengths, respectively, have been observed[32] to enhance EQE from 4.8 to 7.1% for the dual-corrugated structure (20.8% enhancement).

Analogous nanocone arrays in a ZnO layer on ITO with a pitch of 270 nm were observed to increase the output power of blue GaN LEDs on sapphire substrates by 45.6%.[33]

It would have been desirable to have experimental measurements to verify the predictions of these simulations. Although the synthesis of conformally corrugated OLEDs is very challenging, preliminary experimental work by Hippola et al.[22] with triangular lattice nanoarrays of pitch 750−800 nm and a corrugation height of 280−400 nm measured $\eta_{EQE} \sim 50\%$ and enhancement factor of 2.6 relative to a flat glass/ITO device.

https://doi.org/10.1021/acsomega.1c00903
ACS Omega 2021, 6, 9291−9301

Our simulated $\eta_{out} \sim 60.5\%$ (Figure 4a) for pitch $a \sim 800$ nm is very consistent with this measured EQE of $\eta_{EQE} \sim 50\%$, since $\eta_{EQE} > \eta_{out}$ (eq 1), indicating that the product $\gamma \cdot \eta_{s/t} \cdot \eta_\rho \sim 0.82$ (eq 1)—estimating internal losses within the OLED. Additional experiments with a range of pitch values will be very useful to further validate our simulations. The control of light emission by nanoarrays in OLEDs has intriguing analogies to the previously studied modification of emission rates for dipole sources at the surface of photonic crystals or dipoles embedded within the photonic crystal.[34] The enhancement of the photonic densities of states at frequencies near the photonic band edges[35] modifies the Purcell factor analogous to OLEDs.

6. CONCLUSIONS

A critical problem facing OLEDs is the very low outcoupling ($\eta_{out} \sim 20\%$) of light, due to large waveguiding losses in the high-index layers and substrate, and plasmonic losses at the metal cathode. A major scientific initiative is underway to vastly increase the light outcoupling to $\eta_{out} > 70\%$, for OLED lighting applications.

We simulate light outcoupling from novel periodically corrugated OLEDs, which can be grown on a periodically corrugated transparent substrate. Since the emissive layer is also conformally corrugated, theoretical approaches for planar OLEDs cannot be directly utilized. Accordingly, we develop a rigorous scattering matrix theory for light outcoupling in corrugated OLEDs that have corrugated emissive layers, in which vectorial Maxwell's equations are solved for all three polarizations of the incident dipole field. Experimental wavelength-dependent dielectric functions of OLED material layers are utilized.

We find periodically corrugated conformal OLEDS exhibit optimal light outcoupling η_{out} as high as 60−65% over optical wavelengths. This is an enhancement factor of ∼3 to 4 over the flat OLED. Optimal pitch values are between 1000 and 2500 nm, whereas η_{out} is insensitive to corrugation heights ($h > 100$ nm). There is a gradual roll-off in η_{out} for a larger pitch, and a sharper decrease in η_{out} for pitch values smaller than light wavelengths. Near optimal pitch values, periodic corrugations strongly diffract trapped waveguided and plasmonic modes to the air cone, through first-order diffraction. We simulated the spectral power inside the OLED and in the air region, and subdivided the emitted light into outcoupled modes, waveguided modes, and plasmonic losses. Plasmonic losses remain below 10% for all pitch values. There is weak anisotropy in the light emission with the emission plane, due to diffraction from the discrete reciprocal lattice vectors. Our results provide a pathway for experimentally enhancing the OLED outcoupling through growth on periodically substrates, and for improving the brightness and efficiency of white OLEDs for solid-state lighting applications.

■ ASSOCIATED CONTENT

Supporting Information

The Supporting Information is available free of charge at https://pubs.acs.org/doi/10.1021/acsomega.1c00903.

Mathematical and analytical derivation, flat OLEDs results, and wavelength-dependent refractive indices (PDF)

■ AUTHOR INFORMATION

Corresponding Author

Rana Biswas − *Department of Electrical and Computer Engineering, and Microelectronics Research Center and Ames Laboratory and Department of Physics & Astronomy, Iowa State University, Ames, Iowa 50011, United States;* orcid.org/0000-0002-0866-2100; Email: biswasr@iastate.edu

Author

Yu Zhang − *Department of Electrical and Computer Engineering, and Microelectronics Research Center, Iowa State University, Ames, Iowa 50011, United States*

Complete contact information is available at: https://pubs.acs.org/10.1021/acsomega.1c00903

Notes

The authors declare no competing financial interest.

■ ACKNOWLEDGMENTS

The authors very gratefully acknowledge Ruth Shinar and Joseph Shinar for valuable discussions and suggestions as well as for providing experimental measurements on OLEDs. They thank Dennis Slafer (MicroContinuum) for fruitful discussions and Akshit Peer for earlier simulations. This work was supported by the U.S. Department of Energy (DOE) EERE Grants DE-EE0007621 and DE-EE0008724. The authors acknowledge the use of computational resources at the National Energy Research Scientific Supercomputing Center (NERSC), which is supported by the Office of Science of the USDOE under contract no. DE-AC02-05CH11231

■ REFERENCES

(1) Nowy, S.; Krummacher, B. C.; Frischeisen, J.; Reinke, N. A.; Brütting, W. Light extraction and optical loss mechanisms in OLEDs: Influence of the emitter quantum efficiency. *J. Appl. Phys.* **2008**, *104*, No. 123109.

(2) Brütting, W.; Frischeisen, J.; Schmidt, T. D.; Scholz, B. J.; Mayer, C. Device efficiency of organic light-emitting diodes: Progress by improved light outcoupling. *Phys. Status Solidi A* **2013**, *210*, 44−65.

(3) Gather, M. C.; Reineke, S. Recent Advances in Light Outcoupling from White Organic Light-Emitting Diodes. *J. Photonics Energy* **2015**, *5*, No. 057607.

(4) United States Department of Energy Solid State Lighting Multi-year Program Plan, http://energy.gov/eere/ssl/downloads/solid-state-lighting-rd-plan.

(5) Chang, C. H.; Chang, K.-Y.; Lo, Y.-J.; Chang, S.-J.; Chang, H.-H. Fourfold Power Efficiency Improvement in Organic Light-Emitting Devices using an Embedded Nanocomposite Scattering Layer. *Org. Electron.* **2012**, *13*, 1073−1080.

(6) Möller, A.; Forrest, S. R. Improved Light out-coupling in OLEDS employing ordered microlens arrays. *J. Appl. Phys.* **2002**, *91*, 3324−3327.

(7) Park, J. M.; Gan, Z.; Leung, W. Y.; Liu, R.; Ye, Z.; Constant, K.; Shinar, J.; Shinar, R.; Ho, K. M. Soft holographic interference lithography microlens for enhanced organic light emitting diode light extraction. *Opt. Express* **2011**, *19*, A786−A792.

(8) Peer, A.; Biswas, R.; Park, J. M.; Shinar, R.; Shinar, J. Light management in perovskite solar cells and organic LEDs with microlens arrays. *Opt. Express* **2017**, *25*, 10704−10709.

(9) Sun, Y.; Forrest, S. R. Enhanced light out-coupling of organic light-emitting devices using embedded low-index grids. *Nat. Photonics* **2008**, *2*, 483−487.

(10) Slootsky, M.; Forrest, S. Enhancing waveguided light extraction in organic LEDs using an ultra-low-index grid. *Opt. Lett.* **2010**, *35*, 1052−1054.
(11) Qu, Y.; Kim, J.; Coburn, C.; Forrest, S. R. Efficient, Nonintrusive Outcoupling in Organic Light Emitting Devices Using Embedded Microlens Arrays. *ACS Photonics* **2018**, *5*, 2453−2458.
(12) Koo, W. H.; Jeong, S. M.; Araoka, F.; Ishikawa, K.; Nishimura, S.; Toyooka, T.; Takezoe, H. Light extraction from organic light-emitting diodes enhanced by spontaneously formed buckles. *Nat. Photonics* **2010**, *4*, 222−226.
(13) Koo, W. H.; Zhe, Y.; So, F. Direct Fabrication of Organic Light-Emitting Diodes on Buckled Substrates for Light Extraction. *Adv. Opt. Mater* **2013**, *1*, 404−408.
(14) Peng, C.; Liu, S.; Fu, X.; Pan, Z.; Chen, Y.; So, F.; Schanze, K. S. Corrugated Organic Light Emitting Diodes Using Low Tg Electron Transporting Materials. *ACS Appl. Mater. Interfaces* **2016**, *8*, 16192−16199.
(15) Jeon, S.; Lee, S.; Han, K.-H.; Shin, H.; Kim, K.-H.; Jeong, J.-H.; Kim, J.-J. High-Quality White OLEDs with Comparable Efficiencies to LEDs. *Adv. Opt. Mater.* **2018**, *6*, No. 1701349.
(16) Fuchs, C.; et al. Quantitative allocation of Bragg scattering effects in highly efficient OLEDs fabricated on periodically corrugated substrates. *Opt. Express* **2013**, *21*, 16319−16330.
(17) Schwab, T.; Fuchs, C.; Schole, R.; Zakhidov, A.; Leo, K.; Gather, M. C. Coherent mode coupling in highly efficient top-emitting OLEDS on periodically corrugated substrates. *Opt. Express* **2014**, *22*, 7524−7537.
(18) Altun, A. O.; et al. Corrugated OLEDs for enhanced light extraction. *Org. Electron.* **2010**, *11*, 711−716.
(19) Liang, H.; et al. Corrugated organic light-emitting diodes to effectively extract internal modes. *Opt. Express* **2019**, *27*, No. A372.
(20) Youn, W.; Lee, J. W.; Yu, H.; Kim, D. Y. Effect of Refractive Index Contrast on Out-Coupling Efficiency of Corrugated OLEDs using Low-Refractive-Index LiF Interlayer. *ACS Appl. Electron. Mater.* **2020**, *2*, 2218−2223.
(21) Kim, D. W.; Han, J. W.; Lim, K. T.; Kim, Y. H. Highly Enhanced Light-Outcoupling Efficiency in ITO-Free Organic Light-Emitting Diodes Using Surface Nanostructure Embedded HighRefractive Index Polymers. *ACS Appl. Mater. Interfaces* **2018**, *10*, 985−991.
(22) Hippola, C.; Kaudal, R.; Manna, E.; Xiao, T.; Peer, A.; Biswas, R.; Slafer, W. D.; Trovato, T.; Shinar, J.; Shinar, R. Enhanced Light Extraction from OLEDs fabricated on plastic substrates. *Adv. Opt. Mater.* **2018**, *6*, No. 1701244.
(23) Li, Z.-Y.; Lin, L.-L. Photonic band structures solved by a plane-wave based transfer-matrix method. *Phys. Rev. E* **2003**, *67*, No. 046607.
(24) Peer, A.; Biswas, R. Nano-photonic Organic Solar Cell Architecture for Advanced Light Trapping with Dual Photonic Crystals. *ACS Photonics* **2014**, *1*, 840−847.
(25) Furno, M.; Meerheim, R.; Hofmann, S.; Lüssem, B.; Leo, K. Efficiency and rate of spontaneous emission in organic electro-luminescent devices. *Phys. Rev. B* **2012**, *85*, No. 115205.
(26) Egel, A.; Lemmer, U. Dipole emission in stratified media with multiple spherical scatterers: Enhanced outcoupling from OLEDs. *J. Quant. Spectrosc. Radiat. Transfer* **2014**, *148*, 165−176.
(27) Sullivan, K. G.; Hall, D. G. Enhancement and Inhibition of electromagnetic radiation in plane-layered media. 1. Plane wave spectrum approach to modeling classical effects. *J. Opt. Soc. Am. B* **1997**, *14*, 1149−1159.
(28) Tabulated values of the wavelength dependent refractive indices of ITO and Ag are at www.Refractiveindex.info.
(29) Hermann, S.; Gordon, O. D.; Friedrich, M.; Zahn, D.R.T. Optical properties of multilayered Alq3/α-NPD structures investigated with spectroscopic ellipsometry. *Phys. Status Solidi C* **2005**, *2*, 4037−4042.
(30) Sun, Y.; Forrest, S. R. OLEDs with enhanced outcoupling via microlenses fabricated by imprint lithography. *J. Appl. Phys.* **2006**, *100*, No. 073106.
(31) Alnasser, K.; Hassan, S.; Kamau, S.; Zhang, H.; Lin, Y. Enhanced light extraction from organic light emitting diodes by reducing plasmonic loss through graded photonic super-crystals. *J. Opt. Soc. Am. B* **2020**, *37*, 1283−1289.
(32) Bi, Y.-G.; et al. Broadband light Extraction from white OLEDs by employing corrugated metallic electrodes with dual periodicity. *Adv. Mater.* **2013**, *25*, 6969−6974.
(33) Kim, S.; et al. Conformally direct imprinted inorganic surface corrugation for light extraction enhancement of light emitting diodes. *Opt. Express* **2012**, *20*, A713−A721.
(34) Sigalas, M. M.; Biswas, R.; Ho, K.-M. Theoretical Study of dipole antennas on photonic band gap materials. *Microwave Opt. Technol. Lett.* **1996**, *13*, 205−209.
(35) Biswas, R.; Sigalas, M. M.; Ho, K.-M.; Lin, S. Y. Three-dimensional photonic band gaps in modified simple cubic lattices. *Phys. Rev. B* **2002**, *65*, No. 205121.

https://doi.org/10.1021/acsomega.1c00903
ACS Omega 2021, 6, 9291−9301